A SPARSE LINEAR ARRAY APPROACH IN AUTOMOTIVE RADARS USING MATRIX COMPLETION

Shunqiao Sun[1] *and Athina P. Petropulu*[2]

[1]Department of Eeletrical and Computer Engineering, The University of Alabama, Tuscaloosa, AL 35487
[2]Department of Electrical and Computer Engineering, Rutgers University, Piscataway, NJ 08854
E-mail: shunqiao.sun@ua.edu, athinap@rutgers.edu

ABSTRACT

We consider an automotive radar using a sparse linear array (SLA) in the context of multi-input multi-output (MIMO) radar. The key problem in SLA is the selection of the locations of the array elements so that the peak sidelobe level of the virtual SLA beampattern is low. Prior approaches have focused on optimal sparse array design, or use of interpolation techniques for filling the holes in the synthesized SLA before applying digital beamforming for angle finding. In this paper, different from previous efforts, we use matrix completion to complete the corresponding virtual uniform linear array (ULA) before estimating the target angle. In particular, we show that for a small number of targets within the same range-Doppler cell, the Hankel matrix constructed by subarrays of the virtual ULA is low-rank, and thus under certain conditions, can be completed based on the SLA measurements. We derive the coherence properties of the Hankel matrix so that the matrix can be competed via nuclear norm minimization methods. We also demonstrate via examples the effect of various SLA topologies on the identifiability of the Hankel matrix.

Index Terms— automotive radar, FMCW, autonomous driving, sparse linear array, matrix completion

I. INTRODUCTION

Automotive radars for advanced driver assistance systems (ADAS) and autonomous driving are required to have high angle discrimination capability and small package size so that they can be easily integrated into vehicles. Unlike conventional phase arrays whose resolution is proportional to their size, multi-input multi-output (MIMO) radar can meet both high resolution and small size requirements [1]. This is because MIMO radar can synthesize virtual arrays with large apertures using only small number of transmit and receive antennas. This advantage has been exploited by almost all major automotive Tier-1 suppliers in their different types of radar products [2]–[5]. Even with the help of MIMO radar technology, however, the cost of synthesizing a large virtual ULA with half wavelength element spacing can be very high. One way to further reduce the cost without sacrificing angle resolution is to use virtual sparse linear arrays (SLAs), e.g., use a thinned receive ULA. For that reason, SLA technology has been attracting great interest in automotive radar applications [6]–[10].

The idea of SLA is to use a MIMO radar and properly deploy the reduced number of transmit and receive antennas such that the element spacing of the corresponding virtual array is larger than half wavelength, while its aperture is the same as that of a ULA with half wavelength element spacing. The array response of the SLA has missing elements when compared to that of a ULA with the same aperture [6]. However, the irregular spacing of the array elements in SLA introduces grating lobes, which may cause angle ambiguity. Therefore, the key problem in SLA is the selection of the locations of the array elements so that the peak sidelobe level (PSL) of the virtual SLA beampattern is low. As there is no analytical solution to determining the antenna locations that achieve a minimum PSL for a given number of antennas [11], optimal sparse array design has been conducted based on global optimization techniques, such as particle swarm optimization [12]. If the grating lobes of SLAs are low, angle finding can be done via compressive sensing (CS) and sparse signal recovery ideas [13], [14]; this requires to discretize the whole field of view into a fine grid. However, CS suffers from off-grid issues [15] and signal-to-noise ratio (SNR) loss due to the sparse sampling. On the other hand, interpolation or extrapolation techniques have been widely adopted in automotive radars to fill the holes in the syntehsized SLA before applying digital beamforming for angle finding [16], [17]. However, it is difficult to interpolate or extrapolate the holes when the SLAs are irregular, or the number of holes is large.

In this paper, we show that instead of filling the holes of SLAs via interpolation, one could use matrix completion techniques [18], [19] to complete the corresponding virtual ULAs. We show that a Hankel matrix constructed by subarrays of the virtual ULA has a low rank structure. The Hankel matrix corresponding to a virtual SLA can be viewed as a spatially sampled version of the Hankel ULA matrix, thus has missing elements. Under certain conditions, the Hankel matrix can be completed based on the SLA measurements. Once the Hankel matrix is completed, the elements in the virtual ULA can be recovered and high resolution angle finding can be carried out via the matrix pencil method [20], or other subspace based methods, such as ESPRIT and MUSIC. The identifiability of the matrix completion problem depends on the locations of the observed entries of a matrix [21]. Once the problem is identifiable, conditions for matrix completion with high probability using nuclear-norm minimization depend on the coherence properties of the matrix. We derive the coherence properties of the Hankel matrix, and also examine SLA topologies that lead to an identifiable matrix completion problem. In particular, we discuss two SLA topologies: one with irregular element spacing, and the other with uniform element spacing that is larger than half wavelength. The proposed approach avoids the off-grid issue, which is inherent in compressive sensing methods [15]. In addition, it avoids loss of SNR in the array response since the response of all the virtual array elements are recovered.

II. SYSTEM MODEL

Frequency-modulated continuous-wave (FMCW) waveforms are popular in automotive radar as they enable high resolution target

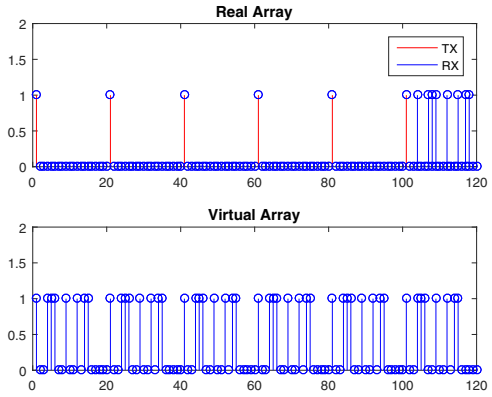

Fig. 1. Example of an automotive radar cascaded with two transceivers. The virtual array has 48 elements.

range and velocity estimation while requiring low cost samplers at the receive antennas [22]. An FMCW waveform is a chirp signal and is transmitted periodically with a certain repetition interval. The target echo is mixed with the transmitted chirp, which results in a complex sinusoid, known as *beat signal*. The frequency of the beat signal is the sum of the range frequency and the Doppler frequency, each containing information about the target range and Doppler. Estimation of the beat frequency is implemented in the digital domain with two fast Fourier transforms (FFTs), i.e., a range FFT (taken on samples obtained within the waveform repetition interval) followed by a Doppler FFT (taken on samples across repetition intervals), after sampling the beat signal with a low-speed analog-to-digital converter (ADC) (hence it's low cost). The targets are first separated in range and Doppler domains. As a result, the number of targets in the same range Doppler bin is typically small, which enables angle finding with sparse sensing techniques, such as compressive sensing [13], [14].

A typical automotive radar transceiver, such as the AWR1243 of Texas Instruments [23], has $M_t = 3$ and $M_r = 4$ antennas. Depending on performance requirement and cost, automotive radar can use one or multiple transceivers to synthesize a SLA for angle finding. Figure 1 shows an example of the real array configuration of an automotive radar which is a cascaded of 2 transceivers, where all transmit and receive antennas are clock synchronized. Let λ denote the wavelength of carrier frequency. In this example, $M_t = 6$ transmit antennas are deployed with uniform spacing of 10λ, while $M_r = 8$ receive antennas are randomly deployed on discretized grid points in an interval of length equal to 10λ. The interval is discretized uniformly with spacing of half wavelength. The transmit antennas transmit FMCW waveform in a way that at each receive antenna the contribution of each transmit antenna can be separated. The latter can be achieved using time domain multiplexing (TDM), or Doppler domain multiplexing (DDM), which effectively introduce waveform orthogonality among the transmitted waveforms (see [22] for details). Therefore, with MIMO radar technology, a virtual SLA with 48 array elements and aperture of 57λ has been synthesized, as shown in Fig. 1. Compared to a ULA with half wavelength spacing and the same aperture, some elements at certain locations of the above virtual SLA are "missing" (denoted by zeros in the virtual array of Fig. 1). However, the SLA approach uses a reduced number of transmit and receive antennas, which saves hardware cost. In addition, SLA helps in reducing the mutual coupling between antenna elements, and thus improves the array calibration performance [24].

The array response at a particular time instance consisting of data obtained at all the $M_t M_r$ virtual receivers and corresponding to the same range-Doppler bin is defined as the *array snapshot*. The SNR in the array snapshot is much higher than that in the beat signal, since energy has been accumulated in both range and Doppler domains via the two FFTs. For example, a range FFT of length N_R combined with a Doppler FFT of length N_D can provide total $10\log_{10}(N_R N_D)$ dB SNR improvement. The high SNR in the array snapshot reduces the DOA estimation error.

III. A NOVEL SPARSE LINEAR ARRAY APPROACH

Suppose an array snapshot contains K targets with direction of arrivals (DOAs) $\theta_k, k = 1, \cdots, K$. Without noise, the SLA response can be written as

$$\mathbf{y}_S = \mathbf{A}_S \mathbf{s}, \tag{1}$$

where $\mathbf{A}_S = [\mathbf{a}_S(\theta_1), \cdots, \mathbf{a}_S(\theta_K)]$ is the steering matrix with $\mathbf{a}_S(\theta_k) = \left[1, e^{j\frac{2\pi}{\lambda} d_1 \sin(\theta_k)}, \cdots, e^{j\frac{2\pi}{\lambda} d_{M_t M_r - 1} \sin(\theta_k)}\right]^T$ and d_i is the spacing of the i-th element of SLA to its reference element. Here, $\mathbf{s} = [\beta_1, \cdots, \beta_K]^T$, where β_k denotes the amplitude associated with the k-th target.

The corresponding virtual ULA with $M = M_t M_r$ array elements and element spacing $d = \lambda/2$ has array response

$$\mathbf{y} = \mathbf{A}\mathbf{s}, \tag{2}$$

where $\mathbf{A} = [\mathbf{a}(\theta_1), \cdots, \mathbf{a}(\theta_K)]$ is the array steering matrix with $\mathbf{a}(\theta_k) = \left[1, e^{j\frac{2\pi}{\lambda} d \sin(\theta_k)}, \cdots, e^{j\frac{2\pi}{\lambda}(M-1) d \sin(\theta_k)}\right]^T$.

When $M = 2N - 1$, $\mathbf{y} \in \mathbb{C}^{2N-1}$ can be divided into N overlapped subarrays of length N. Based on those subarrays, let us formulate a square Hankel matrix $\mathbf{Y} \in \mathbb{C}^{N \times N}$ with $\mathbf{Y}_{ij} = \mathbf{y}_{i+j-1}$ for $i = 1, \cdots, N$ and $j = 1, \cdots, N$ (our approach works in non-square case). The Hankel matrix $\mathbf{Y}$ has a Vandermonde factorization [25], shown below

$$\mathbf{Y} = \mathbf{B}\mathbf{\Sigma}\mathbf{B}^T, \tag{3}$$

where $\mathbf{B} = [\mathbf{b}(\theta_1), \cdots, \mathbf{b}(\theta_K)]$ is the subarray steering matrix with $\mathbf{b}(\theta_k) = \left[1, e^{j\frac{2\pi}{\lambda} d \sin(\theta_k)}, \cdots, e^{j\frac{2\pi}{\lambda}(N-1) d \sin(\theta_k)}\right]^T$ and $\mathbf{\Sigma} = \mathrm{diag}(\beta_1, \cdots, \beta_K)$ is a diagonal matrix. Thus, the rank of Hankel matrix $\mathbf{Y}$ is K if $N > K$.

The Hankel matrix corresponding to an SLA configuration can be viewed as a subsampled version of $\mathbf{Y}$. However, under certain conditions, the missing elements can be fully recovered by solving a relaxed nuclear norm optimization problem conditioned on the observed entries [18]

$$\min \|\mathbf{X}\|_* \quad \text{s.t. } \mathbf{X}_{ij} = \mathbf{Y}_{ij}, \ (i,j) \in \Omega \tag{4}$$

where Ω is the set of indices of observed entries that is determined by the SLA.

Once the matrix $\mathbf{Y}$ is recovered, the full array response is obtained by averaging its anti-diagonal entries. DOAs can be estimated via standard array processing methods based on the array response corresponding to the completed $\mathbf{Y}$.

The conditions of matrix completion are related to the bounds on the coherence of $\mathbf{Y}$, and also the placement of the sampling entries.

III-A. Coherence Properties of Hankel Matrix

Let $\mathbf{U}$ and $\mathbf{V}$ be left and right subspaces of the singular value decomposition (SVD) of $\mathbf{Y} \in \mathbb{C}^{N\times N}$, which has rank K. The coherence of $\mathbf{U}$ (similarly for $\mathbf{V}$) equals [18]

$$\mu(U) = \frac{N}{K} \max_{1\le i\le N} \|\mathbf{U}(i,:)\|^2 \in \left[1, \frac{N}{K}\right], \tag{5}$$

The matrix $\mathbf{Y}$ has coherence with parameters μ_0 and μ_1 if
(**A0**) $\max(\mu(U), \mu(V)) \le \mu_0$ for some positive μ_0.
(**A1**) The maximum element of matrix $\sum_{1\le i\le K} \mathbf{u}_i \mathbf{v}_i^H$ is bounded by $\frac{\mu_1\sqrt{K}}{N}$ in absolute value for some positive μ_1.

It was shown in [18] that if entries of matrix $\mathbf{Y}$ are observed uniformly at random, and there are constants C, c such that if $|\Omega| \ge C \max\left(\mu_1^2, \mu_0^{1/2}\mu_1, \mu_0 N^{1/4}\right) \eta K N \log N$ for some $\eta > 2$, the minimizer to problem (4) is unique and equal to $\mathbf{Y}$ with probability of $1 - cN^{-\eta}$. Therefore, if matrix $\mathbf{Y}$ has a low coherence parameters, it can be completed using a less number of observed entries.

The following Theorem relates the coherence of Hankel matrix $\mathbf{Y}$ to the relative location of targets, the number of targets and N.

Theorem 1. *(Coherence of Hankel Matrix $\mathbf{Y}$): Consider the Hankel matrix $\mathbf{Y}$ constructed from a uniform linear array as presented in Section III and assume the set of target angles $\{\theta_k\}_{k\in\mathbb{N}_K^+}$ consists of almost surely distinct members, with minimal spatial frequency separation $x = \min_{(i,j)\in\mathbb{N}_K^+\times\mathbb{N}_K^+, i\ne j} \frac{d}{\lambda}(\sin\theta_i - \sin\theta_j)$ satisfying $|x| \ge \xi \ne 0$. If $K \le \sqrt{\frac{N}{\beta_N(\xi)}}$ where $\beta_N(\xi) = \frac{1}{N}\frac{\sin^2(\pi N\xi)}{\sin^2(\pi\xi)}$ is the Fejér kernel, the matrix $\mathbf{Y}$ satisfies the conditions (**A0**) and (**A1**) with coherence parameters*

$$\mu_0 \triangleq \frac{\sqrt{N}}{\sqrt{N} - (K-1)\sqrt{\beta_N(\xi)}}, \tag{6}$$

and $\mu_1 \triangleq \mu_0\sqrt{K}$ with probability 1.

Proof. The proof of Theorem 1 can follow the steps in [26], [27] and is omitted due to space limitation. □

The Fejér kernel $\beta_N(x)$ is a periodic function of x. For $d = \lambda/2$, the spatial frequency separation satisfies $|x| \in (0, 1/2]$. If $0 < \xi < 1/N$, it holds that $\beta_N(\xi) = \mathcal{O}\left(\frac{1}{\sqrt{N}}\right)$. Increasing the number of sub-array elements N will decrease μ_0. In the limit w.r.t. N, it holds that $\lim_{N\to\infty} \mu_0 = 1$, which is its smallest possible value.

III-B. Identifiability of Full Array via Matrix Completion

In this section we examine SLA topologies that can guarantee unique completion of the low-rank Hankel matrix $\mathbf{Y}$.

Let's look at an example of two SLA configurations shown in Figure 2 (a). Both SLAs have the same number of array elements and the same aperture size of 3λ. The second SLA is a ULA with element spacing of $d = \lambda$. Assume that there is one target at angle θ. Let $\gamma \triangleq e^{j2\pi\frac{d}{\lambda}\sin\theta}$. The normalized array snapshot of a ULA with aperture size of 3λ is $\mathbf{y} = \left[1, \gamma, \gamma^2, \gamma^3, \gamma^4, \gamma^5, \gamma^6\right]^T$. The array snapshots of the two SLAs are $\mathbf{y}_1 = \left[1, \gamma, *, \gamma^3, *, *, \gamma^6\right]^T$ and $\mathbf{y}_2 = \left[1, *, \gamma^2, *, \gamma^4, *, \gamma^6\right]^T$, where $*$ denotes the missing

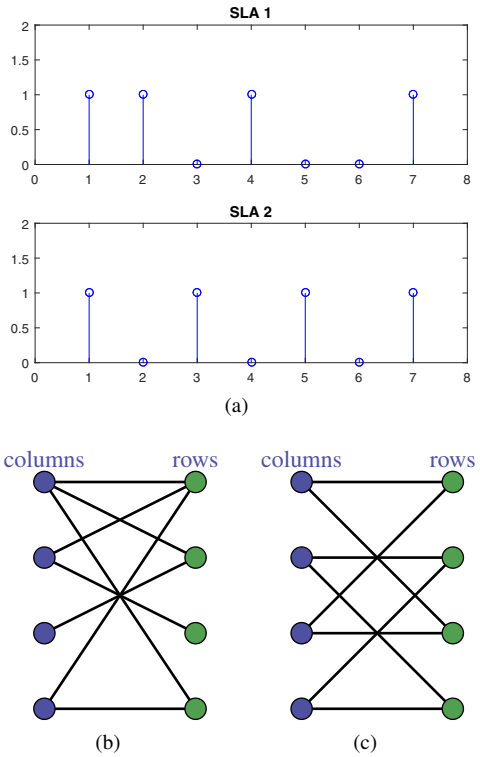

Fig. 2. Examples of SLA: (a) two SLAs and corresponding bipartite graphs (b) $\mathcal{G}_1$ and (c) $\mathcal{G}_2$.

elements. Under the above two different SLAs, the Hankel matrices with missing elements are

$$\mathbf{Y}_1 = \begin{bmatrix} 1 & \gamma & * & \gamma^3 \\ \gamma & * & \gamma^3 & * \\ * & \gamma^3 & * & * \\ \gamma^3 & * & * & \gamma^6 \end{bmatrix}, \mathbf{Y}_2 = \begin{bmatrix} 1 & * & \gamma^2 & * \\ * & \gamma^2 & * & \gamma^4 \\ \gamma^2 & * & \gamma^4 & * \\ * & \gamma^4 & * & \gamma^6 \end{bmatrix}.$$

Matrix $\mathbf{Y}$ is rank one and it can be reconstructed from $\mathbf{Y}_1$ uniquely. However, there would be infinite completions of $\mathbf{Y}$ from $\mathbf{Y}_2$. In a ULA with element spacing $d = \lambda$, there is angle ambiguity which cannot be mitigated via the matrix completion approach.

Let $\mathcal{G} = (V, E)$ be a bipartite graph associated with the sampling operator P_Ω, where $V = \{1, 2, \cdots, N\} \cup \{1, 2, \cdots, N\}$ and $(i,j) \in E$ iff $(i,j) \in \Omega$. Let $\mathbf{G} \in \mathbb{R}^{N\times N}$ be the biadjacency matrix of the bipartite graph $\mathcal{G}$ with $\mathbf{G}_{ij} = 1$ iff $(i,j) \in \Omega$. Note that $P_\Omega(\mathbf{Y}) = \mathbf{Y} \odot \mathbf{G}$, where $\odot$ denotes the Hadamard product. The two bipartite graphs, $\mathcal{G}_1$ and $\mathcal{G}_2$ associated with the two SLAs are shown in Fig. 2, respectively. It can be seen that $\mathcal{G}_1$ is connected, while $\mathcal{G}_2$ is not. For a unique reconstruction of $\mathbf{Y}$, the graph must be connected [21].

The recoverability of a low rank matrix can also be characterized by the spectral gap of graph $\mathcal{G}$, which is defined as the difference between the first two largest singular values of $\mathbf{G}$ [28]. If the spectral gap of matrix $\mathbf{G}$ is sufficient large, the nuclear norm minimization method defined in (4) exactly recovers the low-rank matrix satisfying the conditions (**A1**) and (**A2**). It can be verified that $\mathcal{G}_2$ is a 2-regular graph with $\sigma_1(\mathbf{G}) = \sigma_2(\mathbf{G}) = 2$. Thus the spectral gap of $\mathbf{G}_2$ is zero and $\mathbf{Y}$ cannot be recovered from $\mathbf{Y}_2$.

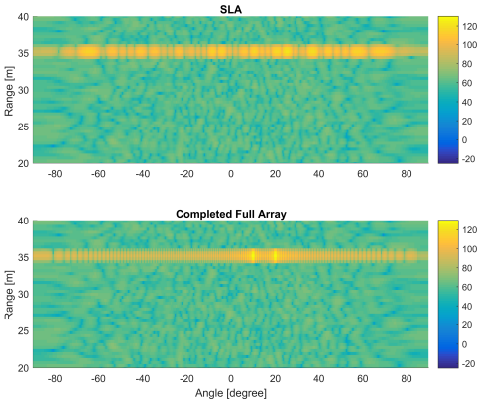

Fig. 3. Range angle spectrum of two stationary targets at range of 35 m with angles of $\theta_1 = 10^\circ$ and $\theta_2 = 20^\circ$.

Let $\mathcal{G}^{-1}_{K+1,K+1}$ denote the complete bipartite graph with $(K+1)\times(K+1)$ vertices minus one edge. The graph $\mathcal{G}$ is called a K-closed bipartite graph, if $\mathcal{G}$ does not contain a vertex set whose induced subgraph is isomorphic to $\mathcal{G}^{-1}_{K+1,K+1}$. In general, as shown in [21], a rank-K matrix can be uniquely completed only if the bipartite graph $\mathcal{G}$ associated with the sampling is K-closable. It was shown in [28] that if Ω is generated from a d-regular graph $\mathcal{G}$ with sufficient large spectra gap, and $d \geq 36C^2\mu_0^2K^2$, then the nuclear norm optimization of (4) exactly recover the low-rank matrix, where C is a constant. It can be seen that if the coherence of $\mathbf{Y}$, i.e. μ_0 defined in Theorem 1 is low, the required number of observation samples or array elements of SLA is less.

IV. NUMERICAL RESULTS

We consider an automotive radar setup of Fig. 1 with FMCW transmit waveforms of bandwidth $B = 350$MHz, corresponding to range resolution of $\Delta R = 0.43$ meters. For one coherent processing, a total of 512 FMCW chirps are transmitted, with chirp duration of $T = 28\mu$s.

We consider two stationary targets at range of 35 meter with DOA of $\theta_1 = 10^\circ$ and $\theta_2 = 20^\circ$. The SNR of the beat signal is set as 0dB. To estimate the range and Doppler of the targets, a range FFT of length 256 and a Doppler FFT of length 512 are implemented on the sampled beat signal for all 48 channels. The 2 FFT operations (range FFT followed by Doppler FFT) not only help separate targets in the range-Doppler domains, but also provide an SNR improvement in the array response of around 51dB corresponding to the same range-Doppler bin.

The SLA shown in Fig. 1 acts as a deterministic sampler of a rank-2 Hankel matrix $\mathbf{Y} \in \mathbb{C}^{N\times N}$ with $N = 60$, which is constructed based on the array response of a ULA with 119 elements. The array response of the SLA is normalized by its first element. Based on the observed SLA response, the Hankel matrix $\mathbf{Y}$ is completed via the singular value thresholding (SVT) algorithm [29]. Let $\hat{\mathbf{Y}}$ denote the completed Hankel matrix. The full ULA response can be reconstructed by taking the average of the anti-diagonal elements of matrix $\hat{\mathbf{Y}}$. The completed full array has aperture size of 59λ. Intuitively, in this simulation setting, matrix

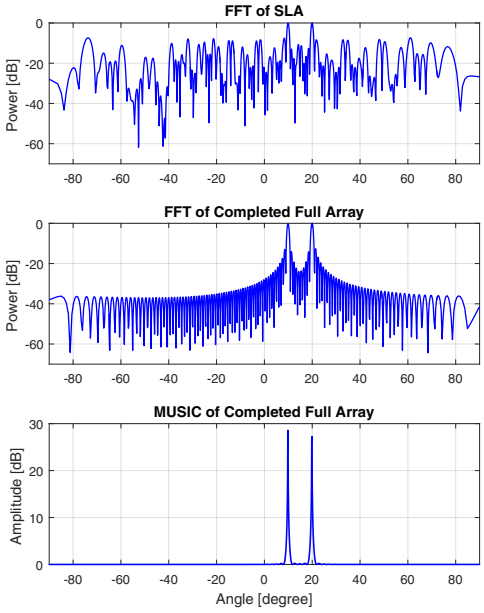

Fig. 4. Comparison of original SLA and completed full array using FFT and MUSIC pseudo spectrum of the array snapshot.

completion contributes around $10\log 10\,(119/48) = 3.94$dB SNR improvement for array processing.

In Fig. 3, we plot the range angle spectrum for the two stationary targets. The two azimuth angle spectra are obtained by applying an FFT to the original SLA with the holes filled with zeros, and the full array completed via matrix completion, respectively. It can be found that it is difficult to detect the two targets in azimuth directions under the original SLA due to its high grating lobes. On the contrary, there are two clear peaks corresponding to correct range and azimuth locations in the range angle spectrum of the completed full array. The comparison of SLA and the completed full array via FFT and MUSIC is shown in Fig. 4. With spatial smoothing [30], we divide the completed full array into overlapped subarrays of length $N = 60$ and formulate a covariance matrix $\mathbf{R} \in \mathbb{C}^{N\times N}$. The MUSIC algorithm is then applied to $\mathbf{R}$. It can be found that FFT of SLA generates two peaks corresponding to the correct azimuth directions at a cost of high grating lobes, which are suppressed under the completed full array. The MUSIC pseudo spectrum based on the completed full array response yields sharp peaks corresponding to the correct azimuth directions.

V. CONCLUSIONS

We have demonstrated the idea of using SLAs for high resolution, low cost DOA estimation in automotive radar applications. By properly designing SLAs, and completing the Hankel matrix of the SLA response, DOA estimation does not suffer from grating lobes. We have derived the Hankel matrix coherence properties and investigated the conditions of array element placement in SLA such that the matrix is recoverable. The proposed approach has been verified via simulation. Our future work will include design of SLAs that meet the desirable identifiability and recoverability conditions for the Hankel matrix.

VI. REFERENCES

[1] J. Li and P. Stoica, "MIMO radar with colocated antennas," *IEEE Signal Process. Mag.*, vol. 24, no. 5, pp. 106–114, 2007.

[2] I. Bilik and *et al.*, "Automotive MIMO radar for urban environments," in *Proc. IEEE Radar Conference*, Philadelphia, PA, May 2016.

[3] S. Alland and J. Searcy, "Radar system and method of digital beamforming," U.S. Patent 2009/0085800, April 2, 2009.

[4] M. Wintermantel, "Radar system with improved angle formation," U.S. Patent 2011/0074621, Mar. 31, 2011.

[5] M. Schoor and *et al.*, "Method for operating a MIMO radar," U.S. Patent 2014/0347211, Nov. 27, 2014.

[6] C. Schmid, R. Feger, C. Wagner, and A. Stelzer, "Design of a linear non-uniform antenna array for a 77-GHz MIMO FMCW radar," in *Proc. IEEE MTT-S International Microwave Workshop on Wireless Sensing, Local Positioning, and RFID*, Cavtat, Croatia, Sept. 2009.

[7] C. A. Alcalde, "Radar system and method for virtual antenna signals," U.S. Patent 9 664 775 B2, May 30, 2017.

[8] Z. Li and C. A. Alcalde, "Angle finding for a detector having a paired staggered array," U.S. Patent 2018/0267555 A1, Sept. 20, 2018.

[9] S. Alland, "MIMO antenna with improved grating lobe characteristics," U.S. Patent 2015/0253419 A1, Sept. 10, 2015.

[10] J. Searcy and S. Alland, "MIMO antenna with elevation detection," U.S. Patent 9 541 639 B2, Jan. 10, 2017.

[11] R. Feger, C. Wagner, S. Schuster, S. Scheiblhofer, H. Jager, and A. Stelzer, "A 77-GHz FMCW MIMO radar based on an SiGe single chip transceiver," *IEEE Trans. Microw. Theory Tech.*, vol. 57, no. 5, pp. 1020–1035, 2009.

[12] N. Jin and Y. Rahmat-Samii, "Advances in particle swarm optimization for antenna designs: Real-number, binary, single-objective and multiobjective implementations," *IEEE Trans. Antennas Propag.*, vol. 55, no. 3, pp. 556–567, 2007.

[13] Y. Yu, A. P. Petropulu, and H. V. Poor, "MIMO radar using compressive sampling," *IEEE J. Sel. Topics Signal Process.*, vol. 4, no. 1, pp. 146–163, 2010.

[14] Y. Yu, S. Sun, R. N. Madan, and A. P. Petropulu, "Power allocation and waveform design for the compressive sensing based MIMO radar," *IEEE Trans. Aerosp. Electron. Syst.*, vol. 50, no. 2, pp. 898–909, 2014.

[15] Y. Chi, L. L. Scharf, A. Pezeshki, and A. R. Calderbank, "Sensitivity to basis mismatch in compressed sensing," *IEEE Trans. Signal Process.*, vol. 59, no. 5, pp. 2182–2195, 2011.

[16] S. Alland and *et al.*, "Virtual radar configuration for 2D array," U.S. Patent 9 869 762, Jan. 16, 2018.

[17] T. Spreng and *et al.*, "Wideband 120 GHz to 140 GHz MIMO radar: System design and imaging results," in *Proc. European Microwave Conference (EuMC)*, Paris, France, Sept. 2015.

[18] E. J. Candès and B. Recht, "Exact matrix completion via convex optimization," *Foundations of Computational Mathematics*, vol. 9, no. 6, pp. 717–772, 2009.

[19] E. J. Candès and T. Tao, "The power of convex relaxation: Near-optimal matrix completion," *IEEE Trans. Inf. Theory*, vol. 56, no. 5, pp. 2053–2080, 2010.

[20] Y. Hua and T. K. Sarkar, "Matrix pencil method for estimating parameters of exponentially damped/undamped sinusoids in noise," *IEEE Trans. Acoust., Speech, Signal Process.*, vol. 38, no. 5, pp. 814–824, 1990.

[21] F. Király and R. Tomioka, "A combinatorial algebraic approach for the identifiability of low-rank matrix completion," in *Proc. 29th Intl. Conference on Machine Learning (ICML)*, Edinburgh, Scotland, UK, June 2012.

[22] S. Sun, A. P. Petropulu, and H. V. Poor, "MIMO radar for ADAS and autonomous driving: Advantages and challenges," *IEEE Signal Process. Mag.*, under review, 2019.

[23] Texas Instruments, "AWR1243 single-chip 77- and 79-GHz FMCW transceiver," datasheet, 2017.

[24] A. Ganis and *et al.*, "A portable 3-D imaging FMCW MIMO radar demonstrator with a 24x24 antenna array for medium-range applications," *IEEE Trans. Geosci. Remote Sens.*, vol. 56, no. 1, pp. 298–312, 2018.

[25] J. Ying, J. F. Cai, D. Guo, G. Tang, Z. Chen, and X. Qu, "Vandermonde factorization of Hankel matrix for complex exponential signal recovery—application in fast NMR spectroscopy," *IEEE Trans. Signal Process.*, vol. 66, no. 21, pp. 5520–5533, 2018.

[26] S. Sun and A. P. Petropulu, "Waveform design for MIMO radars with matrix completion," *IEEE J. Sel. Topics Signal Process.*, vol. 9, no. 8, pp. 1400–1411, 2015.

[27] D. S. Kalogerias and A. P. Petropulu, "Matrix completion in colocated MIMO radar: Recoverability, bounds & theoretical guarantees," *IEEE Trans. Signal Process.*, vol. 62, no. 2, pp. 309–321, 2014.

[28] S. Bhojanapalli and P. Jain, "Universal matrix completion," in *Proc. 31st Intl. Conference on Machine Learning (ICML)*, Beijing, China, June 2014.

[29] J. F. Cai, E. J. Candès, and Z. Shen, "A singular value thresholding algorithm for matrix completion," *SIAM J. Optim.*, vol. 20, no. 2, pp. 1956–1982, 2010.

[30] T. Shan, M. Wax, and T. Kailath, "On spatial smoothing for direction-of-arrival estimation of coherent signals," *IEEE Trans. Acoust., Speech, Signal Process.*, vol. 33, no. 4, pp. 506–811, 1985.